JOURNAL OF SPACECRAFT AND ROCKETS
Vol. 32, No. 1, January–February 1995

# Nonreactive Viscous Solver for Hypersonic Flows over Recessed Cone with Injection

C. H. Tai*
*Chung Cheng Institute of Technology, Taiwan, Republic of China*
and
Y. K. Lee†
*Combined Service Forces, Taipei 115, Taiwan, Republic of China*

**A nonreactive two-species flow in which the gas is injected from the downstream wall of the recess on a hypersonic sharp cone has been investigated by solving the steady full Navier–Stokes equations. The discretization methods have combined Roe's scheme and multiblock grids for accurate calculations. The species equation has been included in order to simulate the flowfield by injecting different gases. The flow structure and cooling effect has been investigated at $M_\infty = 6.0$. The flow structure of the recess has been shown by the perfect gas computational results to be significantly affected by injecting cool species gases. An optimal injection rate for the cooling effect has also been shown to exist on the downstream wall of the cone. The cooling effect of injecting helium has been shown to be better than nitrogen and air for both isothermal and adiabatic wall conditions.**

## Nomenclature

$C_i$ = mass fraction of species $i$
$D_{ij}$ = pertinent binary diffusion
$d$ = characteristic molecular diameter
$E$ = total energy
$H^*$ = total enthalpy
$h_i$ = enthalpy of species $i$
$J$ = injection parameter, $\rho_{\text{inj}} u_{\text{inj}} A_{\text{inj}} / \rho_\infty u_\infty A_{\text{rw}}$
$k$ = thermal conduction
$L$ = total length of cone
$M$ = molecular weight, Mach number
$N$ = atomic number for a molecular
$P$ = pressure
$Pr$ = Prandtl number
$q$ = energy flux
$\bar{q}$ = normalized heat flux, Eq. (25)
$R$ = gas constant
$Re$ = Reynolds number per foot, $\rho_\infty V_\infty / \mu_\infty$
$T$ = temperature
$\bar{T}$ = temperature ratio, $T/T_\infty$
$T_0$ = stagnation temperature
$V$ = streamwise velocity
$u, v, w$ = Cartesian velocity components in $x, y, z$ direction
$X$ = mole fraction
$\gamma$ = ratio of specific heat
$\mu$ = viscosity coefficient
$\bar{\mu}$ = viscosity ratio, $\mu/\mu_\infty$
$\tau$ = shear stress
$\rho$ = density

*Subscripts*

$i, j$ = various chemical species
inj = injection conditions
$m$ = region of mixing
$w$ = wall conditions
$rw$ = wall of recess
$x, y, z$ = Cartesian coordinates
$d$ = coefficient of $\Omega$ for diffusively
$\kappa$ = coefficient of $\Omega$ for conductivity
$\mu$ = coefficient for $\Omega$ for viscosity
$\infty$ = freestream conditions

*Superscript*

$\hat{}$ = Roe average

Received May 1, 1992; revision received March 9, 1993; accepted for publication Oct. 3, 1993. 

*Associate Professor, Department of Mechanical Engineering.
†Engineer, Ballistic Research Center, Ordnance Production Service, P. O. Box 90582-28.

## Introduction

THE investigation of heat transfer to hypersonic re-entry vehicles has long been a very interesting problem for aeronautics and ballistics. This problem is of practical importance because the aerodynamic heating at hypersonic speeds is significant and represents a major factor limiting flight conditions for nonabrading surfaces. One way of reducing this high operational surface temperature is by cutting a recess out of the vehicle and injecting cool gas into it. The growing cost of wind-tunnel testing, particularly for the hypersonic regime, and the difficulty of accurately simulating the full-scale flow in ground-based experimental facilities makes an experimental-based design of a slot cooling system for a hypersonic vehicle very difficult. Computational preliminary research becomes very important for investigating this kind of problem.

Many papers have dealt with hypersonic cone research.[1,2,3] Few, however, have dealt with the hypersonic cone with gas injection from a recess section. Only one paper regarding this experimental field exists.[4] Because of limited computational capacity, numerical simulation in the computational field has been confined in the past to inviscid problems or simple geometry models.[5] No papers have dealt with hypersonic cavity-flow research. A computer code solving the steady full Navier–Stokes equations for a nonreactive mixture of two perfect gases is developed in this paper for analyzing the flowfield of an axisymmetric, recessed, sharp cone by injecting helium and nitrogen with an arbitrary injection rate. It has provided a numerical tool for simulating this kind of problem in considerable detail and at a lower cost than wind-tunnel testing.

The numerical algorithm using the explicit multistage, upwind flux-difference split scheme (Roe's scheme)[6,7] is shown in this study to provide reasonable supersonic or hypersonic flow characteristics. It also simulates the boundary layer and shock more accurately than the Beam–Warming scheme[8] or MacCormack's scheme.[9] Multiblock grids have been utilized to include the physical space of the cone and recess.

The present study analyzes the laminar flowfield at $M_\infty = 6.0$. The boundary condition in this paper concerns the isothermal wall

or adiabatic wall specification. The flow properties are reasonably assumed to be an ideal gas model because the vibration energy of the gas is not significant at $M_\infty = 6.0$ (Refs. 10 and 11). The cold species gases are injected into the recess through a vent located in the bottom wall of the recess near the afterwall. The flow structure and the cooling effect resulting from different injection rates of the cold species gases were investigated. The computational results, which were achieved by using an HP 9000/700 computer, show that reasonable properties of hypersonic flow in an axisymmetric recessed cone with different injection rates have been obtained. An optimal injection rate for the cooling effect on the downstream wall of the cone also exists for various species of injection gases.

## Governing Equation

Properly simulating all aerodynamic properties over the recessed, sharp cone is the ultimate goal. Simulating the species flow to solve the axisymmetric, full Navier–Stokes equations is considered by the developed code. The governing equation can be represented in strong conservation form as

$$\frac{\partial \bar{U}}{\partial t} + \frac{\partial \bar{F}}{\partial x} + \frac{\partial \bar{G}}{\partial y} + \frac{\partial \bar{H}}{\partial z} = 0 \tag{1}$$

where $x$, $y$, and $z$ are the Cartesian coordinates and

$$\bar{U} = \begin{bmatrix} \rho \\ \rho u \\ \rho v \\ \rho w \\ \rho E \\ \rho c_i \end{bmatrix} \quad \bar{F} = \begin{bmatrix} \rho u \\ \rho u^2 + p - \tau_{xx} \\ \rho uv - \tau_{xy} \\ \rho uw - \tau_{xz} \\ \rho uH^* - u\tau_{xx} - v\tau_{xy} - w\tau_{xz} + q_x \\ \rho uC_i - \rho D_{ij}\nabla C_i \end{bmatrix}$$

$$\bar{G} = \begin{bmatrix} \rho v \\ \rho uv - \tau_{xy} \\ \rho v^2 + p - \tau_{yy} \\ \rho vw - \tau_{yz} \\ \rho vH^* - u\tau_{xy} - v\tau_{yy} - w\tau_{yz} + q_y \\ \rho vC_i - \rho D_{ij}\nabla C_i \end{bmatrix} \tag{1a}$$

$$\bar{H} = \begin{bmatrix} \rho w \\ \rho uw - \tau_{xz} \\ \rho uv - \tau_{yz} \\ \rho w^2 + p - \tau_{zz} \\ \rho wH^* - u\tau_{xz} - v\tau_{yz} - w\tau_{zz} + q_z \\ \rho wC_i - \rho D_{ij}\nabla C_i \end{bmatrix}$$

This code is developed in a three-dimensional form and is used here for solving an axisymmetric problem. All the formulas have remained in a three-dimensional form.

The mass diffusion of species $i$ through a mixture for the species continuity equation is also driven by pressure and temperature gradients. The concentration gradients due to $\nabla P$, pressure diffusion, and due to $\nabla T$, thermal diffusion, are small compared with the mass diffusion.[11] Consequently, pressure and temperature diffusion are neglected in the present gasdynamic simulation. Neglecting the heat and pressure flux in the energy equation provides the transport of heat. This is expressed by Fourier's law of heat conduction and transport of enthalpy due to mass diffusion:

$$q = -\kappa \nabla T + \sum_i \rho_i U_i h_i \tag{2}$$

where $U_i$ is the diffusion velocity of species $i$, and $\kappa$ is the thermal conduction.

In the governing equation of two species for the transport phenomenon in the mixing region, the viscosity $\mu_m$ and thermal conduction $\kappa_m$ can be obtained from Wilke's rule[11]:

$$\mu_m = \sum_i \frac{X_i \mu_i}{\sum_j X_j \phi_{ij}} \tag{3}$$

$$\kappa_m = \sum_i \frac{X_i \kappa_i}{\sum_j X_j \psi_{ij}} \tag{4}$$

where $\mu_i$ and $\kappa_i$ are the coefficients of viscosity and conduction of individual species $i$, which can be obtained from Ref. 11:

$$\mu_i = 2.6693 \times 10^{-5} \frac{\sqrt{TM_i}}{d_i^2 \Omega_\mu} \tag{5}$$

$$\kappa_i = \mu_i \left( \hat{C}_\rho + \frac{5R}{4M_i} \right) \tag{6}$$

and

$$\hat{C}_p = \left[ \frac{5 + 2(N_i - 1)}{2} \right] \frac{R}{M_i}$$

and in Eq. (3)

$$\phi_{ij} = \frac{1}{\sqrt{8}} \left( 1 + \frac{M_i}{M_j} \right)^{-1/2} \left[ 1 + \left( \frac{\mu_i}{\mu_j} \right)^{1/2} \left( \frac{M_j}{M_i} \right)^{1/4} \right]^2 \tag{7}$$

and in Eq. (4)

$$\psi_{ij} = \frac{1}{\sqrt{8}} \left( 1 + \frac{M_i}{M_j} \right)^{-1/2} \left[ 1 + \left( \frac{\kappa_i}{\kappa_j} \right)^{1/2} \left( \frac{M_j}{M_i} \right)^{1/4} \right]^2 \tag{8}$$

The pertinent binary diffusion $D_{ij}$ can be obtained from Fick's law[11]:

$$D_{ij} = 0.0018583 \frac{\sqrt{T^3 \left( \frac{1}{M_i} + \frac{1}{M_j} \right)}}{P d_{ij}^2 \Omega_{d,ij}} \tag{9}$$

where the dummy subscripts $i$ and $j$ denote the various chemical species. The equations for $\Omega_\mu$, $\Omega_\kappa$, $\Omega_{d,ij}$ are collision integral that give the variation of an effective collision diameter as a function of temperature. Values for $\Omega_{\mu'} \Omega_{\kappa'} \omega_{d,ij}$ are obtained from Refs. 11 and 12.

The governing equations are completed by the equation of state that uses the ideal gas law with a specific heat ratio of 1.4 for air and nitrogen, and 1.6667 for helium, respectively. The mixture specific heat ratio and mass can be obtained from

$$\gamma_m = 1 + \sum_i \frac{C_i}{M_i} \Big/ \sum_i \frac{C_i}{M_i(\gamma_i - 1)} \tag{10}$$

$$M_m = 1 \Big/ \sum_i \frac{C_i}{M_i} \tag{11}$$

The Navier–Stokes equations can be expressed in an integral form as a finite volume with an enclosing surface. The integral form can be expressed in terms of the changes in the average state $U$ in the finite volume. The surface integral becomes a sum of fluxes over the six faces of a hexahedron. Equation (1) can be written in the normal flux form as

$$\Delta \tilde{V} \frac{d\bar{U}}{dt} + \sum_{n=1}^{6} F_n \Delta A_n = 0 \tag{12}$$

where $\Delta A_n$ is the area vector of the cell surface and $F_n$ is the flux normal to the cell surface, $F_n = \bar{F} \cos\alpha + \bar{F} \cos\beta + \bar{F} \cos\gamma$, and $\cos\alpha$, $\cos\beta$, $\cos\gamma$ are the directional cosines of the $n$th faces.

## Boundary Condition

The inner boundary at the cone and recess (except the injection area) is computed as the no-slip condition, i.e. $V_x = V_y = 0$. For the location of injection, the temperature of injection gas is assumed as the freestream value, i.e., $T_{inj} = T_\infty$. The injection rate of species gas is defined as $J = \rho_{inj} u_{inj} A_{inj} / \rho_\infty u_\infty A_{rw}$, where $\rho_{inj} u_{inj} / \rho_\infty u_\infty$ is the ratio of the mass flow rate of the injected gas to the mass flow rate in the freestream, and $A_{inj}/A_{rw} = 0.135$ is the ratio of the surface area of the injection to the projected area of the ringlike

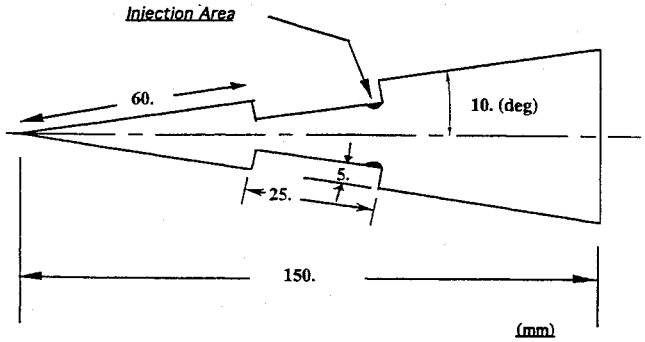


**Fig. 1 Model geometry of axisymmetric cone and recess.**

recess at the aft face (Fig. 1). A characteristic injection boundary condition based on Riemann invariants has been employed by using the pressure $p$ of the computational domain with an assumption of subsonic injection. It is the same specification as $\partial P/\partial n = 0$. Therefore, the density $\rho_{\text{inj}}$ and velocity $u_{\text{inj}}$ of the injection flow can be calculated. The injection velocity vector is normal to the bottom of the recess.

An adiabatic or isothermal wall has been considered. Temperature $T_w$ is the given wall temperature here for an isothermal wall specification. The mass fraction of species $i$ in a chemically reacting flow is one of the dependent variables for a catalytic wall in which chemical reactions are catalyzed at a finite rate. The gradient of mass fraction at the wall is then obtained from Ref. 11 as the following:

$$(\dot{w}_c)_i = \rho D_{ij} \left(\frac{\partial C_i}{\partial y}\right)_w \tag{13}$$

where $\dot{w}_c$ denotes mass of species $i$ lost at the surface per unit area per unit time because of a surface catalyzed chemical reaction. Noncatalytic wall is the topic to be studied, where no reaction occurs at the wall. From Eq. (13)

$$0 = \rho D_{ij}\left(\frac{\partial C_i}{\partial y}\right)_w \qquad 0 = \left(\frac{\partial C_i}{\partial y}\right)_w \tag{14}$$

Equation (14) is the noncatalytic boundary condition used here.

For an adiabatic wall condition, the specification is no heat flux from the wall to the fluid, i.e., the energy flux for the adiabatic wall in the $y$ direction, $q_y$, must be equal to zero at the wall:

$$\left(\kappa \frac{\partial T}{\partial y} + \sum_i D_{ij}\rho_i \frac{\partial C_i}{\partial y}\right)_w = 0 \tag{15}$$

The adiabatic wall condition for a noncatalytic wall can be simplified to

$$\left(\frac{\partial T}{\partial y}\right)_w = 0 \tag{16}$$

According to the far field of the cone, a characteristic analysis based on Riemann invariants is used to determine the values of the flow variable on the outer boundary of the grid. This analysis correctly accounts for wave propagation in the far field, which is important for rapid convergence to steady state.

The multiblock strategy is applied here. Restated, the computation has been implemented by alternately iterating block-by-block. The boundary condition on the interface of the two blocks is calculated from the last iteration step of the other block.

## Numerical Algorithm

Considering the advantage of natural numerical dissipation, the upwind scheme used for solving the Euler or Navier–Stokes equations has become the procedure of choice for providing better stability properties and greater accuracy.[7,13] Such techniques as multigrid strategy, vector and parallel architecture, and local grid refinement are also considered for use; with these methods the explicit scheme is preferable. The explicit Roe flux-difference splitting scheme,[7,10,14,15] which can be applied to the conservation law and can accurately represent the boundary layer, is chosen as the particular upwind method used here.

Equation (1), when looking for the conservative form of this equation, can be discretized as

$$\frac{dU}{dt} + \frac{1}{\nabla \tilde{V}} \sum_{n=1}^{6} F_n \Delta A_n = 0 \tag{17}$$

from which the flux vectors can be written as the sum of an inviscid and a viscous/conductive part:

$$F_n = F_n^i + F_n^\mu \tag{18}$$

The inviscid fluxes and the viscous fluxes are respectively approximated by Roe's scheme and the central difference method.

The basic method of inviscid flux computation is essentially the same for both grid-aligned and grid-independent schemes. It is based on Roe's approximate Riemann solver[16]:

$$\begin{aligned} F_n^i &= F_n^i(U_{R'}, U_L) \\ &= \tfrac{1}{2}\left\{F_n^i(U_R) + F_n^i(U_L)\right\} - \tfrac{1}{2}\left|A(U_{R'}, U_L)\right|(U_R - U_L) \\ &= \tfrac{1}{2}\left\{F_n^i(U_R) + F_n^i(U_L)\right\} - \tfrac{1}{2}\left|A(\hat{U})\right|\Delta U \\ &= \tfrac{1}{2}\left\{F_n^i(U_R) + F_n^i(U_L)\right\} - \tfrac{1}{2}R\left| \wedge \right|\Delta V \end{aligned} \tag{19}$$

where $U_L$ and $U_R$ are the left and right interface states and $\Delta U = U_R - U_L$. Matrix $A$ is the Jacobian matrix of $F(U)$. Matrix $\Lambda$ is the diagonal matrix of eigenvalues.

The Roe average-state variables for a mixture of species are $\hat{\rho} = \sqrt{\rho_R \rho_L}$ and

$$\hat{q} = \frac{q_L\sqrt{\rho_L} + q_R\sqrt{\rho_R}}{\sqrt{\rho_L} + \sqrt{\rho_R}} \tag{20}$$

where $q = [u, v, w, H, c_i]^T$, and the "hats" refer to Roe average. The speed of sound can be obtained from

$$\hat{C} = \sqrt{(\hat{r} - 1)\left(\hat{H} - \frac{\hat{u}^2}{2}\right)} \tag{21}$$

where

$$\hat{r} = 1 + \sum_i \frac{\hat{C}_i}{M_i} \Big/ \sum_i \frac{\hat{C}_i}{M_i(\hat{\gamma}_i - 1)} \tag{22}$$

Matrix $R$ is composed of the right eigenvector of $A$, and $\Delta V = R^{-1}\Delta U$. For example, in one-dimensional flow

$$R = \begin{bmatrix} 1 & 1 & 1 & 0 \\ u + c & u & u - c & 0 \\ H + uc & u^2/2 & H - uc & B \\ C_i & 0 & 0 & 1 \end{bmatrix} \tag{23}$$

where $B$ is the corrective term for the species equation. Such as

$$B = \frac{(\hat{r} - 1)}{\hat{r}} h M_m \left[\frac{1}{(r_1 - 1)M_1} - \frac{1}{(r_2 - 1)M_2}\right] \tag{24}$$

where $h = \sum c_i h_i$. For the $i$ species mixture, $i - 1$ species equations are required; the value of $B_i$ for the $i$ species mixture becomes

$$B_i \frac{(\hat{r} - 1)}{\hat{r}} h M_m \sum_i^n \frac{\Delta c_i}{(\gamma_i - 1)M_i} \tag{25}$$

## Grid System

In general, there are two injection means of cooling the downstream surface in hypersonic flow: 1) providing swept slot injection

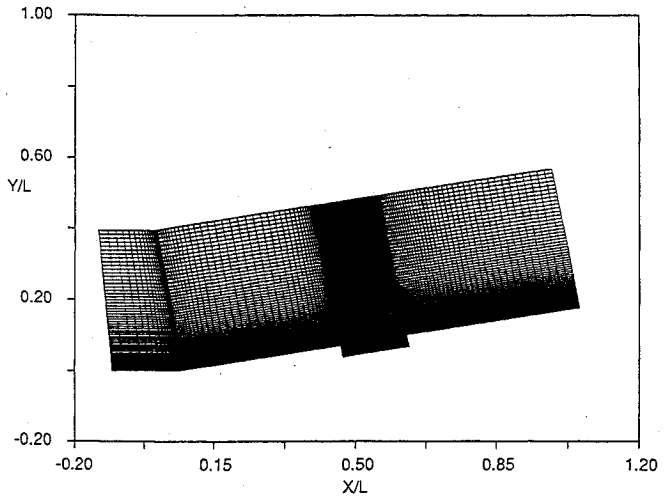


**Fig. 2 Multiblock grids for cone and recess.**

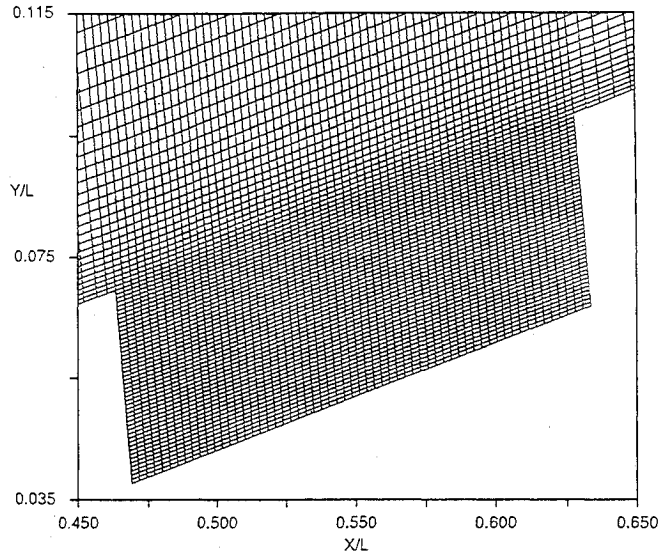


**Fig. 3 Multiblock grids for the recess.**

to the flow[3] and 2) cutting a recess orthogonal to the vehicle, and blowing cooling air from it.[4] Because the flow structure for a hypersonic vehicle is very sensitive to its configuration, the discontinuous boundary of a swept slot will cause a significant disturbance in flight. However, the cavity that is orthogonally cut in the spacecraft still has a stable flow structure in hypersonic velocity. It is provided by a shear layer that forms on the open face of the recess and covers the recess. Therefore, we chose method 2 as the practical approach for analysis.

The proposed model used here is an axisymmetric sharp-nosed cone with a semivertex angle $\Theta = 10$ deg and the length $L = 150$ mm (Fig. 1). A ringlike recess with a length $\ell = 25$ mm and depth $\hbar = 5$ mm is orthogonally cut out at the location of 60 (mm) from the nose tip.

Using an elliptic or hyperbolic-type grid generation to produce a single grid that includes the cone and recess is impractical, because the axisymmetric cone with an annular recess has a complex configuration. Multiblock grids shown in Fig. 2 are used in this study. The algebraic grids used over the cone employ the Robert function[17] to cluster grid points in the boundary-layer region and in the recess (Fig. 3). The grid distance near the wall is approximately $1.0 \times 10^{-3}$.

For the isothermal wall condition, the dimensionless heat flux of the wall has been taken as

$$\bar{q} = \frac{\bar{\mu}}{RePr(\gamma - 1)M_\infty^2}\left(\frac{\partial \bar{T}}{\partial \bar{n}}\right) \tag{26}$$

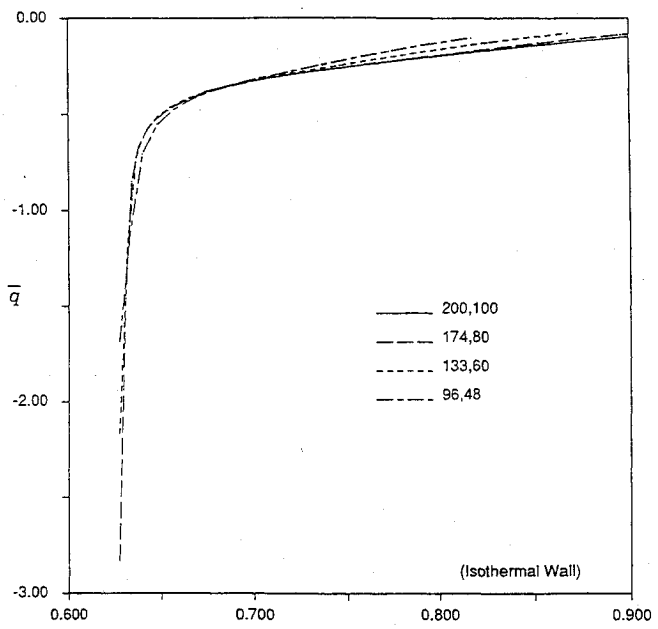


**Fig. 4 Surface heat flux at the downstream wall of the cone using different grid sizes: $M_\infty = 6.0, Re/\text{foot} = 5.6 \times 10^5, J = 0.022$ (nitrogen).**

with $Re$ and $Pr$ denoting the Reynolds number and Prandtl number, and $\gamma$ is the specific heat ratio. The dimensionless viscosity and temperature is defined as $\bar{\mu} = \mu/\mu_\infty$ and $\bar{T} = T/T_\infty$. The surface heat flux for the case in which the number of cells is $200 \times 100$ for the cone and $92 \times 76$ for the recess is shown in Fig. 4. The result is essentially the same as the case in which the grid numbers used were $174 \times 80$ on the cone and $82 \times 60$ on the recess as shown in Fig. 4. It proved that this grid was adequate for investigating the cooling effect on the downstream wall of this model.

## Results and Discussion

Numerical results for an annular recess on a hypersonic cone in laminar flow with different injection gases were obtained for the following conditions:

$$M_\infty = 6.0, \qquad \gamma_\infty = 1.4, \qquad Re/\text{foot} = 5.6 \times 10^5$$

$$T_\infty = T_{\text{inj}} = 200\,K, \qquad A_{\text{inj}}/A_{rw} = 0.135$$

$$J = 0.0, 0.0073, 0.01, 0.022, 0.044, 0.085$$

**Isothermal Wall ($T_w = 951.2$ K)**

For the case of a recessed sharp cone without injection, the recess is filled with air and the flow pattern forming in the recess during supersonic flow is known as an "open recess flow."[18] This is the case provided that the ratio of the length of the recess to its depth $\ell/\hbar <$ 15. A circulatory flow supplied with energy from the viscous mixing layer exists in the recess (Fig. 5). The mass fraction distribution, for helium injected from the bottom of the recess near the rear wall ($J = 0.0073$), is shown in Fig. 6. The helium concentrates in the recess with a small distribution downstream of the cone. Much of the injection gas flows to the downstream field of the cone for the injection rate $J = 0.085$ case (Fig. 7). Several temperature profiles for various injection rates are shown in Fig. 8. Temperatures near the wall are not significantly reduced (Fig. 8) for small (0.0073) or large (0.085) injection rates. However, a significant reduction of temperature near the wall occurs for the case of injection rate $J =$ 0.01. A vortex has formed at the position near the recess for large injection rates (Fig. 9). For large injection rates, the cool injected helium absorbs energy from the freestream high-temperature air in the vortex and will cool the temperature near the recess; however, the downstream temperature near the wall is not significantly reduced.

Temperature contours for various injection gases with $J = 0.022$ are presented in Fig. 10. Temperature ratios less than 1.0 are found near the injection region of the recess associated with the expansion of the injected gas. For the case of helium injection (Fig. 10), the

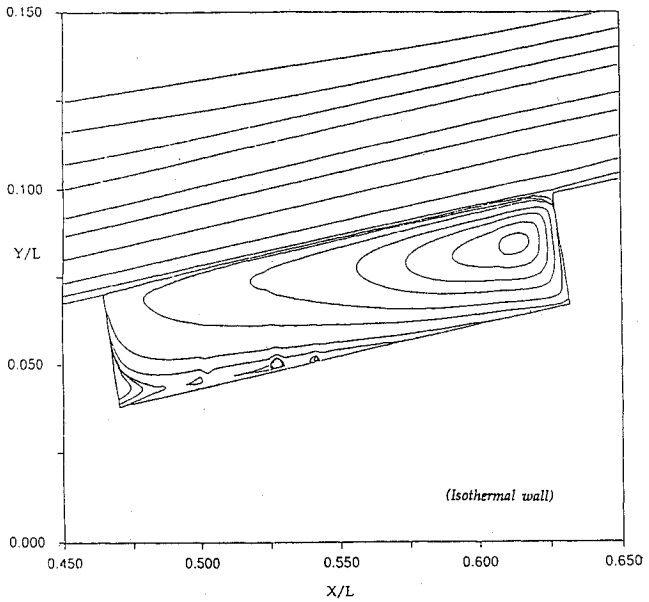


**Fig. 5 Streamlines over cone and recess: $J = 0.00$ (isothermal wall).**

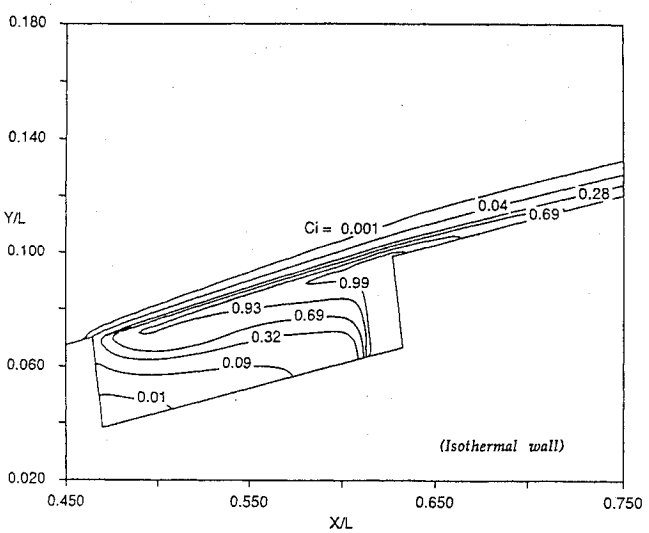


**Fig. 6 Mass fraction for flow over cone and recess (helium): $J = 0.0073$ (isothermal wall).**

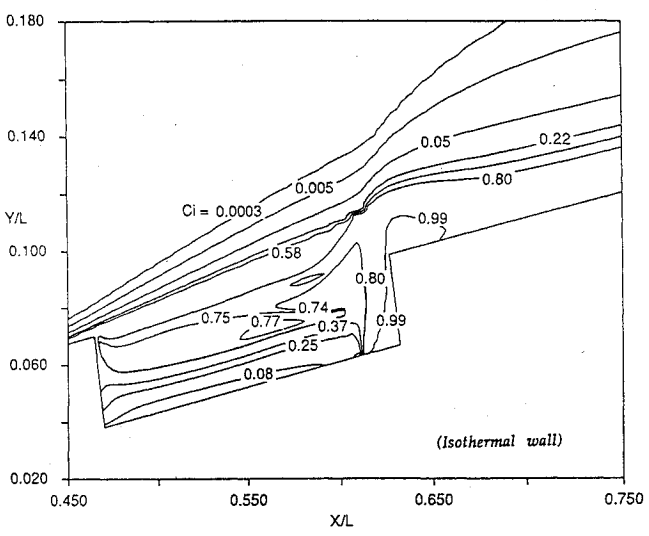


**Fig. 7 Mass fraction for flow over cone and recess (helium): $J = 0.085$ (isothermal wall).**

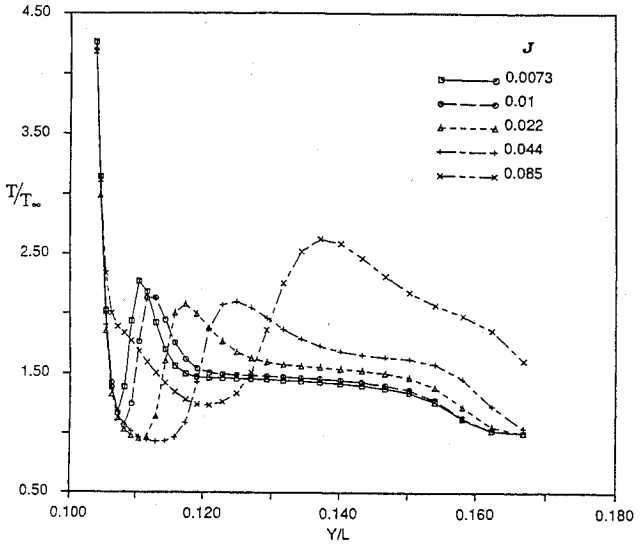


**Fig. 8 Temperature profiles for various injection rates (helium: isothermal wall).**

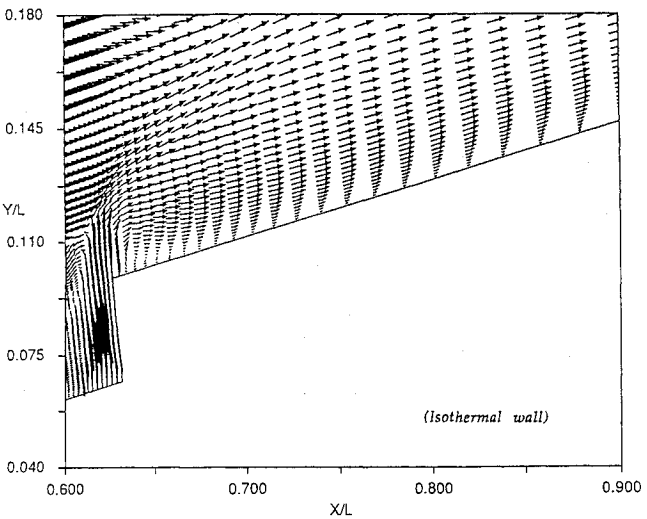


**Fig. 9 Velocity vector plot for flow over cone and recess (helium): $J = 0.085$ (isothermal wall).**

expansion phenomena and low-temperature regime are significant, resulting from the lower molecular weight of helium.

From Eq. (26), the negative heat flux indicates the temperature of the isothermal wall is higher than temperature of the flowfield near the wall (i.e., heat transfer from wall to flow); conversely, the flow delivers energy as heat to the wall for the case of positive heat flux. It is desired that injection gases will cool down the downstream temperature near the wall, requiring a negative heat flux. The large injection rate of cool gas naturally promotes the cooling effect. However, the downstream cooling effect of $J = 0.044$ and 0.085 is less effective than that of $J = 0.022$ (Fig. 11). Large injection rates will greatly absorb energy from the viscous shear layer over the recess and reduce the downstream cooling effect. Thus, it is reasonable that an optimum injection value will promote better cooling effectiveness near the downstream wall. Consequently, for the vehicle requirement of minimizing weight, the optimal injection rate is 0.022 for air injection. Injection of helium (Fig. 12) indicates the downstream cooling effect near the wall is not dependent on injection rate. The heat transfer fluxes with $J = 0.022$ for various injection gases are shown in Fig. 13. The heat fluxes for nitrogen injection are similar to results using air because the molecular weights are almost equal. Figure 13 indicates nitrogen injection has the best cooling effect near the downstream wall.

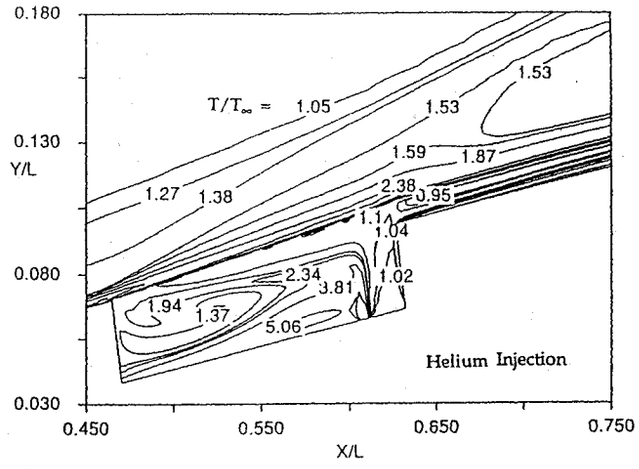


a)

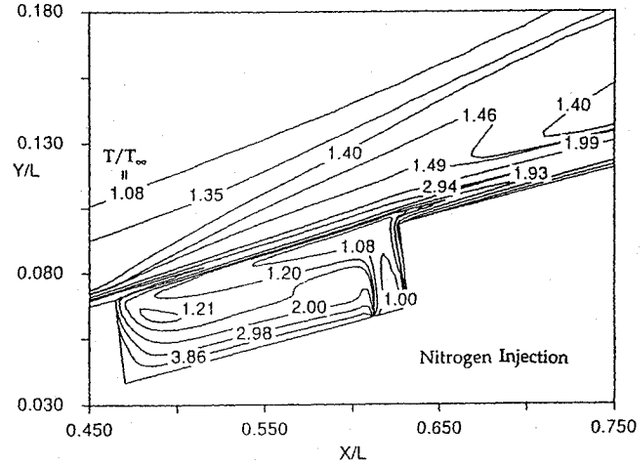


b)

**Fig. 10 Temperature contours for different injection gases: $J = 0.022$ (isothermal wall).**

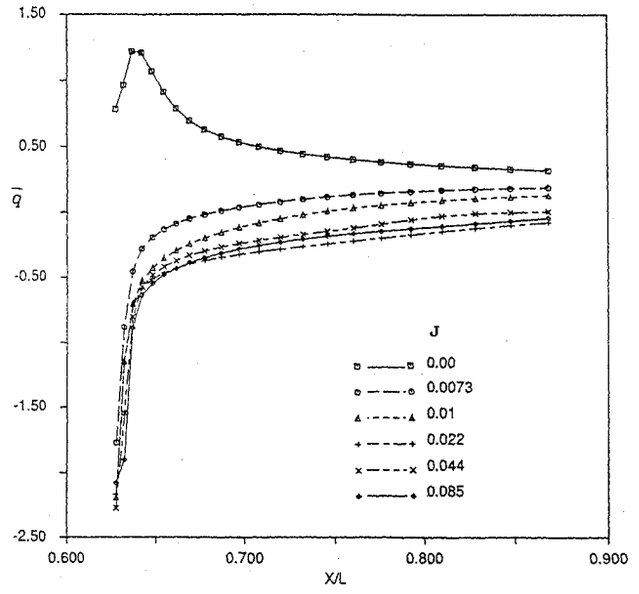


**Fig. 11 Surface heat fluxes at the downstream wall of the cone for different injection rates (air:isothermal wall).**

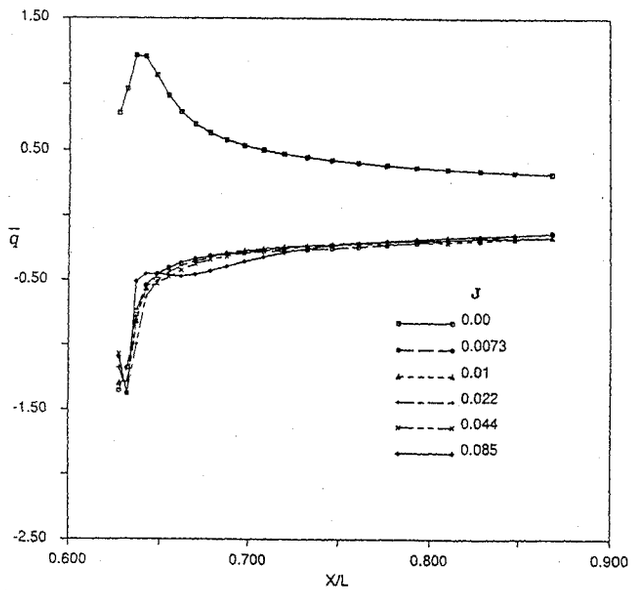


**Fig. 12 Surface heat fluxes at the downstream wall of the cone for different injection rates (helium:isothermal wall).**

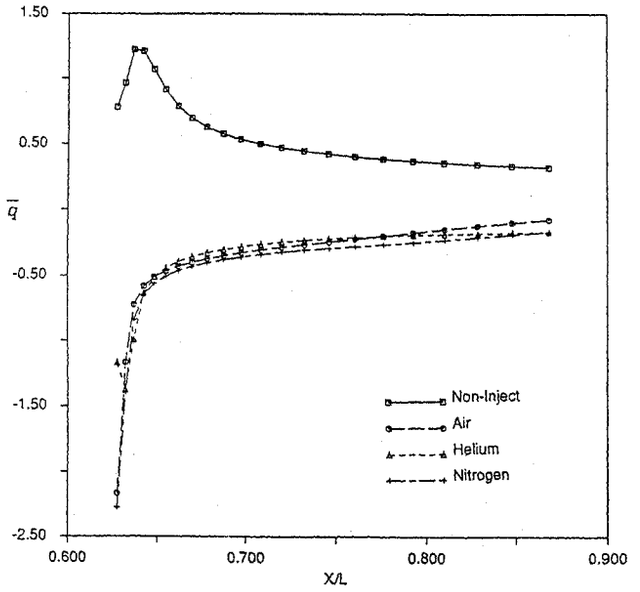


**Fig. 13 Surface heat fluxes at the downstream wall of the cone for different injection gases: $J = 0.022$ (isothermal wall).**

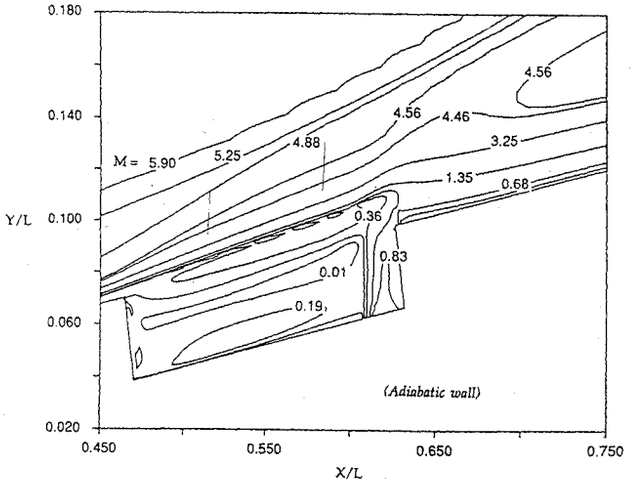


**Fig. 14 Mach number contours for flow over cone and recess (helium): $J = 0.044$ (adiabatic wall).**

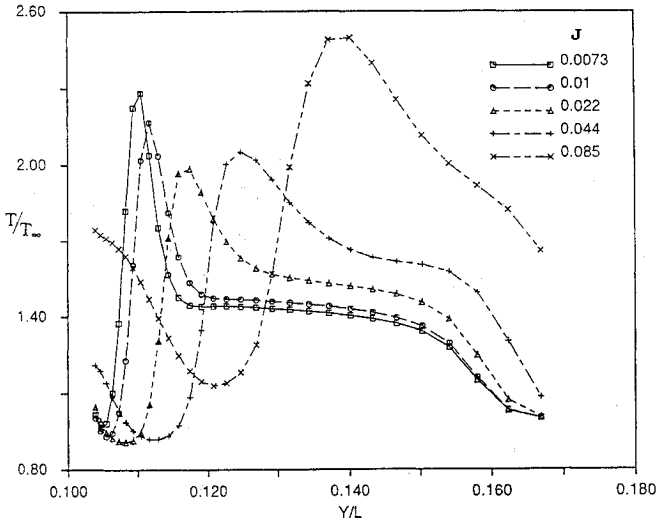


Fig. 15 Temperature profiles for various injection rates (helium: adiabatic wall).

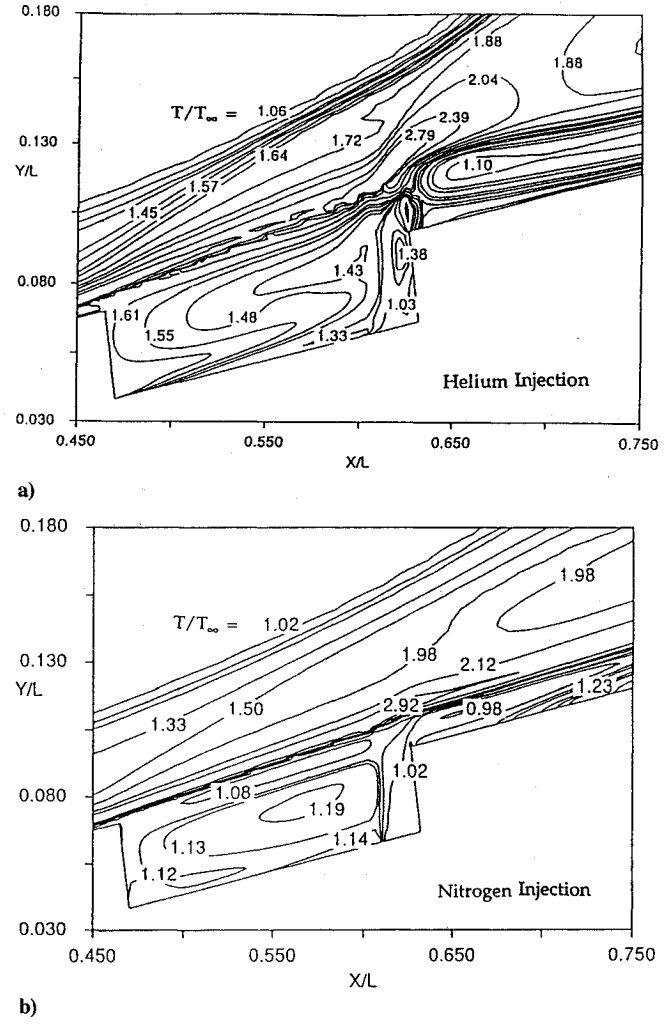


Fig. 16 Temperature contours for different injection gases: $J = 0.085$ (adiabatic wall).

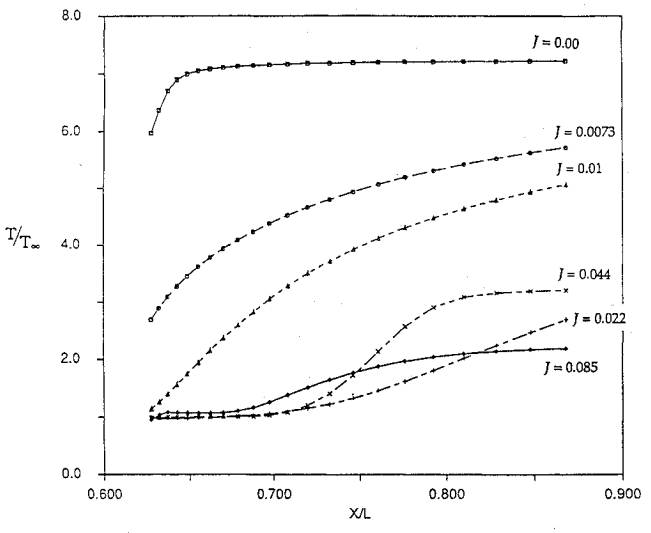


Fig. 17 Surface temperatures at the downstream wall of the cone for different injection rates (air:adiabatic wall).

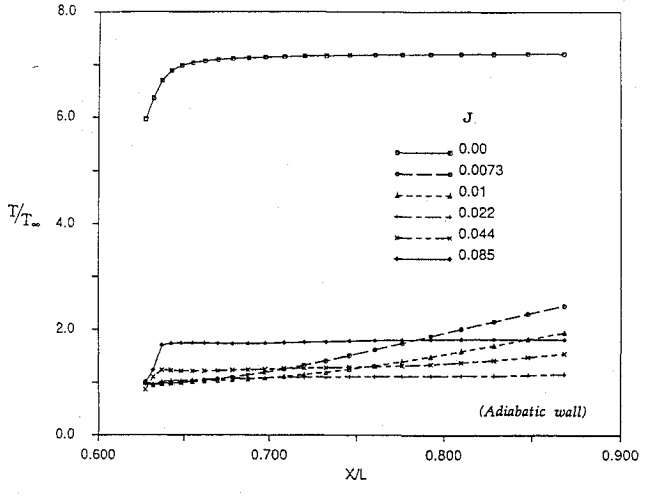


Fig. 18 Surface temperatures at the downstream wall of the cone for different injection rates (helium:adiabatic wall).

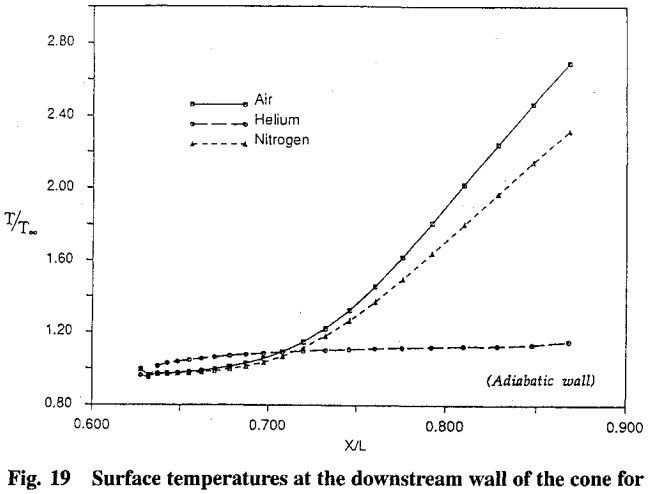


Fig. 19 Surface temperatures at the downstream wall of the cone for different injection gases: $J = 0.022$ (adiabatic wall).

### Adiabatic Wall

The March number contours for helium injection at $J = 0.044$ with an adiabatic wall are shown in Fig. 14. The oblique shock and expansion waves are noted. The cells under the viscous shear layer indicate that the injection gas is obviously mixing with the boundary layer. The temperature profiles are shown in Fig. 15 for various helium injection rates. Low injection rates imply a thin, cool regime near the wall; large injection rates promote a thick, cool regime, but with less reduction of the wall temperature.

For the adiabatic wall condition, the temperature contours of various injection gases for $J = 0.085$ are presented in Fig. 16. A large region for the temperature ratio less than 1.0 is shown for the large injection rate of nitrogen. As the mass flow rate of injecting helium and nitrogen has been specified, the light molecular weight

of helium increases its injection velocity and encourages the energy transfer. Therefore, the temperature ratio contours of helium injection (Fig. 16) are more dispersed than for nitrogen.

The large injection rate of cold air obviously reduces the temperature of the downstream wall (Fig. 17). However, the surface temperature for $J = 0.085$ is above the levels for $J = 0.022$. This is also true for cases using the isothermal wall condition. The optimal injection rate is still at a value of 0.022 to provide the vehicle with the minimum weight. For the cases of helium injection (Fig. 18), low surface temperature are shown, and the optimal injection rate is also 0.022. The same trend of surface temperature for injecting air and nitrogen has been obtained with an optimum value of $J = 0.022$, as shown in Fig. 19. The surface temperature for helium injection are significantly different. Because the helium injection case presents the lowest surface temperature, it can be chosen as the preferred injection gas.

## Conclusion

An effective analysis tool for the study of injecting foreign species cooling flows at hypersonic speed has been developed and demonstrated. The full Navier–Stokes equations, including species equations have been solved using the explicit multistage, upwind flux-difference split scheme (Roe's scheme). The multiblock grids have, as a result of this complex configuration, been used for including the physical space of the axisymmetric cone and the annular recess from which the gas is injected.

The flow structure and cooling effect have been studied for $M_\infty = 6.0$ and Reynolds number of $5.6 \times 10^5$ per foot for the hypersonic recessed sharp-nosed cone with various species gases and injection rates. Results were obtained for the flow structure with arbitrary injection gases. Considering the goals of obtaining minimum weight of the spacecraft and prevention of high surface temperature at hypersonic speed, an injection rate of cool gas that causes the optimal cooling effect on the downstream wall of the cone was obtained. On the basis of injection rate, results for the adiabatic and isothermal wall boundary conditions indicate injecting helium is more effective than nitrogen and air in regard to the downstream cooling effect near the wall.

Experimental data for hypersonic cavity flow with injection of the type considered in this analysis are limited. The measured data in a recent study by Borovoy et al.[4] is inconsistent. Therefore, no available data exist with which the present numerical predictions can be compared. However, the present analysis can be treated as a theoretical basis for qualitatively evaluating the phenomena of hypersonic cavity flow with various species injection gas. A well-designed and carefully conducted experiment for the system considered here would be appropriate.

## References

[1]Nicoll, K. M., "A Study of Laminar Hypersonic Cavity Flows," *AIAA Journal,* Vol. 2, No. 9, 1964, pp. 1535–1541.

[2]Berry, C. T., Vas, T. E., and Bogdonof, S. M., "An Experimental Investigation of Laminar Heat Transfer to Cones at Hypersonic Speeds," Aerospace Research Laboratories, ARL 72-0159, OH, Nov. 1972.

[3]Jerry, N. H., Aubrey, M. C., and Dennis, M. B., "Downstream Influence of Sweep Slot Injection in Hypersonic Turbulent Flow," NASA TN-D-8506, Aug. 1977.

[4]Borovoy, V. Y., Marinichenko, S. K., and Skuratov, A. S., "Heat Transfer in an Annular Recess on a Sharp Cone Operating in Hypersonic Flow With and Without Injection of Gas," *Fluid Mechanics-Soviet Research,* Vol. 17, No. 5, 1988, pp. 26–33.

[5]Sacks, S., "Computation of The Skin-Friction and Heat Transfer on a Sharp Cone in Axisymmetric Turbulent Hypersonic Flow," Naval Ordnance Laboratory, NOL TR 73-79, MD, April 1973.

[6]Roe, P. L., "Discrete Models for The Numerical Analysis of Time-dependent Multidimensional Gas-dynamics," *Journal of Computational Physics,* Vol. 63, 1986, pp. 458–476.

[7]van Leer, B., Thomas, J. L., Roe, P. L., and Newsome, R. W., "A Comparison of Numerical Flux Formulas for the Euler and Navier-Stokes Equations," AIAA Paper 87-1104, 1987.

[8]Beam, R. M., and Warming, R. F., "An Implicit Finite-Difference Algorithm for Hyperbolic System in Conservation Law Form," *Journal of Computational Physics,* Vol. 22, 1976, pp. 87–110.

[9]MacCormack, R. W., "The Effect of Viscosity in Hypervelocity Impact Cratering," AIAA Paper 69-354, 1969.

[10]Hirsch, C., *Numerical Computation of Internal and External Flows*, Vol. 1, Wiley, New York, 1989, pp. 503–512.

[11]Anderson, J. D., Jr., *Hypersonic and High Temperature Gas Dynamic*, McGraw-Hill, New York, 1989.

[12]Bird, R. B., Stewart, W. E., and Lightfoot, E. N., *Transport Phenomena*, Wiley, New York, 1960.

[13]Mulder, and van Leer, B., "Experiments with Implicit Upwind Methods for the Euler Equations," *Journal of Computational Physics,* Vol. 59, 1985, pp. 232–246.

[14]Roe, P. L., "Approximate Riemann Solvers, Parameter Vector, and Difference Schemes," *Journal of Computational Physics,* Vol. 43, 1981, pp. 357–372.

[15]van Leer, B., Tai, C. H., and Powell, K. G., "Design of Optimally Smoothing Multi-Stage Scheme for the Euler Equations," *Proceedings of the AIAA Ninth Computational Fluid Dynamics Conference*, AIAA, Washington, DC, 1989.

[16]van Leer, B., "Upwind-Difference Methods for Aerodynamic Problems Governed by the Euler Equations, in Large-Scale Computations in Fluid Mechanics," *Lectures in Applied Mathematics,* Vol. 22, 1985, pp. 327–336.

[17]Anderson, D. A., Tannehill, J. C., and Pletcher, R. H., *Computational Fluid Mechanics and Heat Transfer*, McGraw-Hill, New York, 1984, pp. 247–255.

[18]Chang, P. K., *International Series of MonoGraphs in Interdisciplinary and Advanced Topics in Science and Engineering—Separation of Flow*, Pergamon, New York, 1970, pp. 296–311.